Forming Limit Diagram Prediction of AA6061-T6 Sheet Using a Microscopic Void Growth Model

Hao H. Nguyen[1], Trung N. Nguyen[2], and Hoa C. Vu[1(✉)]

[1] Department of Engineering Mechanics, Faculty of Applied Science, Ho Chi Minh City University of Technology, 268 Ly Thuong Kiet Street, District 10, Ho Chi Minh City, Vietnam
nguyenhuuhao@tdnu.edu.vn, vuconghoa@hcmut.edu.vn
[2] School of Mechanical Engineering, Purdue University, West Lafayette, IN 47907, USA
trungnguyen@purdue.edu

Abstract. In this paper, a fracture ductile criterion based on the micro-void growth mechanism in metallic material was employed to predict the forming limit diagram (FLD) of AA6061-T6 aluminum alloy sheet. The constitutive model is implemented through a user-defined subroutine in Abaqus/Explicit software. The material parameters were identified via the tensile tests and calibrated by the inverse engineering. The seven Nakajima deep drawing tests are conducted to obtain various plastic deformation states of material. The limit strain values of FLD are then attained by the linear best fit and cross-section approaches.

Keywords: Forming limit diagram · Micro-void growth · McClintock model · Micro-crack mechanism

1 Introduction

The forming limit diagram (FLD) of sheet metal is always of interest in forming process under plastic deformation to avoid waste. The AA6061-T6 aluminum alloy sheet is known as industrial material with its light weight and high strength. Therefore, finding a suitable model to accurately predict its FLD curve is still need to continuous.

Theory of FLD is developed over the decades. The pioneers in this field can be mentioned as Keeler [1] and Goodwin [2]. Marciniak-Kuczynski (M-K) [3] and Marciniak et al. [4] continued it and proposed a model based on an inconsistency in sheet metal that is able to predict localized necking. Today, it is known as M-K theory model and commonly used to estimate FLD of sheet metal [5, 6]. Beside the FLD theory prediction, the Nakajima test model is also applied widely in experiment and numerical simulation to determine the forming limit curve. According to the ISO 12004-2:2008 standard, the Nakajima test is usually conducted for the several specimens to present the strain paths of sheet from uniaxial to biaxial stretched loading state. In the Nakajima test, a hemispherical punch with relatively large diameter

V.H. Duy et al. (eds.), *AETA 2017 - Recent Advances in Electrical Engineering and Related Sciences: Theory and Application*, Lecture Notes in Electrical Engineering 465,
https://doi.org/10.1007/978-3-319-69814-4_98

(approximation of 100 mm) is used to deform the notched specimen until occurred failure. The limit strains are determined by alternative time-dependent or cross section methodology.

To predict the FLD through the ductile fracture models, the phenomenological approaches are usually used. The original metal material is usually containing the second phase particles or/and inclusions. Once the metallic material under deformation lead to the nucleation, growth and coalescence of voids that it is root of ductile damage. An early search in this field has performed by McClintock [7] for growth of cylindrical void in rigid-plastic media. For spherical void growth has found by Rice and Tracey [8].

In this work, a modified McClintock criterion that based on ellipsoidal void growth is adopted, the Dung ductile fracture criterion [9] integrated with the continuum damage mechanics (CDM) theory to evaluate the applicability of the Dung model for investigating the forming limit diagram of AA6061-T6 aluminum alloy. The fracture model was implemented by a user-defined material subroutine (VUMAT) of Abaqus/Explicit software. The Nakajima specimens were taken to conduct the deep drawing process. The FLD is predicted using the linear best fit and cross-section approaches.

2 Ductile Fracture Model

To describe the softening phenomenon of material from the beginning of the plastic deformation to the final failure, a damage variable coupled yield rule is used in this work.

$$\Phi\left(\boldsymbol{\sigma}_{ij}, \sigma_f, D\right) = \sigma_e - w(D)\sigma_f = 0 \tag{1}$$

σ_e is von Mises equivalent stress

$$\sigma_e = \sqrt{\frac{3}{2}\mathbf{s}_{ij} : \mathbf{s}_{ij}} \tag{2}$$

$\mathbf{s}_{ij}(i,j = 1,2,3)$ denotes deviatoric stress tensor and σ_f denotes flow stress of the matrix material.

$w(D) = 1 - D^{\beta}$ is the ductile damage function with β is a softening exponent.

D is the damage variable,

$$D = \frac{1}{D_{crit}} \int_0^{\bar{\varepsilon}_f^p} dD = 1 \tag{3}$$

dD is the evolution rate of damage variable. This work adopted a modified McClintock ductile fracture criterion that based on the ellipsoidal void growth in von Mises matrix material [9, 10].

For the ellipsoidal void, there are three critical accumulated damage variables in i (i = 1, 2, 3) directions.

$$dD_i = \left\{ \frac{\sqrt{3}}{(1-n)} \sinh\left[\frac{\sqrt{3}(1-n)}{4} \frac{\sigma_i + \sigma_j + \sigma_k}{\sigma_f} \right] \cdot \cosh\left[\frac{\sqrt{3}(1-n)}{4} \frac{\sigma_j - \sigma_k}{\sigma_f} \right] + \frac{3}{4} \frac{\sigma_i - \sigma_j - \sigma_k}{\sigma_f} \right\} d\bar{\varepsilon}^p \tag{4}$$

The damage accumulated criterion of ellipsoidal void growth:

$$D = \max(D_i)_{(i=1,2,3)} \tag{5}$$

The subscripts i = 1, 2, 3; j = 2, 3, 1; k = 3, 1, 2; respectively, $d\bar{\varepsilon}^p$ and $\bar{\varepsilon}_f^p$ is equivalent ductile strain rate and plastic strain at fracture of matrix material, respectively. $\sigma_{i,j,k}$ denotes the principal stress components.

3 Numerical Implementation

Assuming that the matrix material obeys von Mises material, the von Mises yield criterion coupled with damage variable would be implemented by using "cutting-plane" algorithm [11, 12]. The basic steps in the numerical procedure for iteratively integrating the elasto-plastic constitutive equations are given in Fig. 2.

4 Experimental Work

The experimental works adopted in this section to identify the mechanical behavior of AA6061-T6 aluminum alloy. The specimens to be designed and tested according to the ASTM-E8 standard [13].

Tensile tests were accomplished with a thin sheet that it's nominal thickness of 2 mm. Having least three dog-bone specimens on each direction of the rolling, transverse and 45° to rolling direction have used. The initial length of the gage marks is 50 mm for all tests. The geometry and dimension of dog-bone specimen are given in Fig. 1.

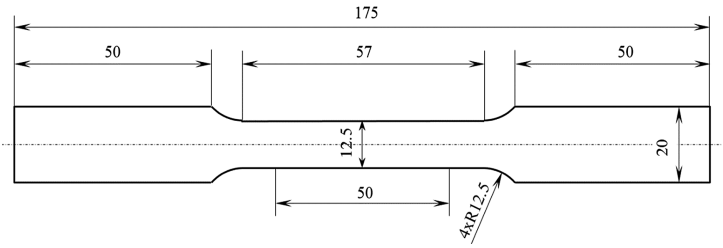

Fig. 1. ASTM-E8 specimen (unit: mm)

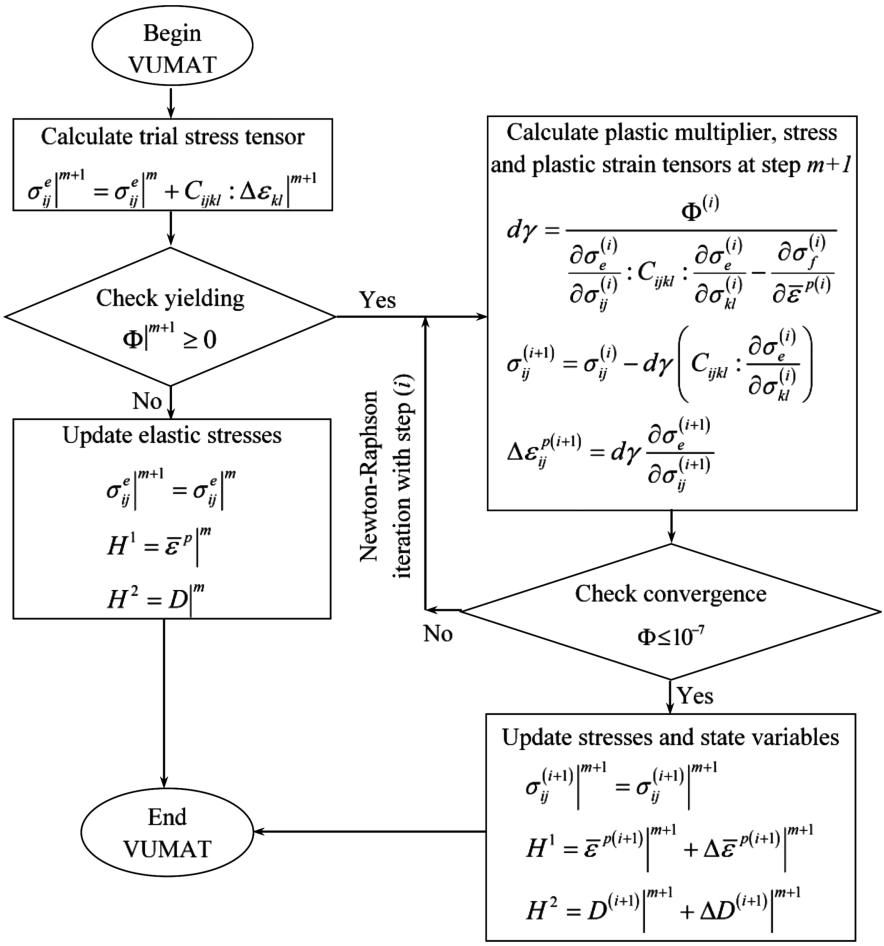

Fig. 2. Flow chart of stress integration algorithm

After tensile tests, the mechanical properties of AA6061-T6 aluminum alloy are given in Table 1 and the true strain-stress curve is given in Fig. 3.

Assuming that the matrix material obeys isotropic hardening rule, the Swift model is used to fit the hardening parameters as follow,

$$\sigma_f = K(\varepsilon_0 + \bar{\varepsilon}^p)^n \tag{6}$$

where K and ε_0 are material constants, n hardening exponent.

Table 1. The mechanical properties of AA6061-T6 aluminum alloy

Parameters	Young's modulus (E)	Yield stress (σ_0)	Poisson's ratio (v)
Value	74.6 GPa	244 MPa	0.314

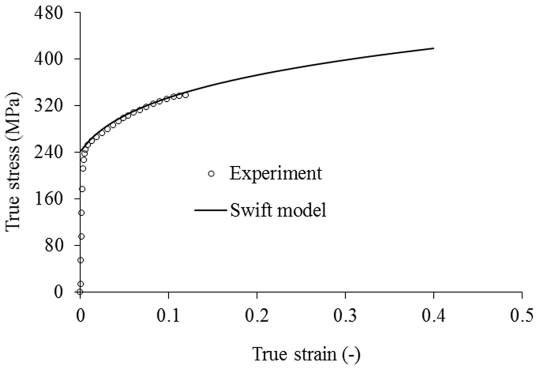

Fig. 3. True strain-stress curve

Fitting true strain-stress curve, the hardening parameters (K, ε_0, n) is obtained as Table 2.

Table 2. The material parameters of AA6061-T6 aluminum alloy

Parameters	K	ε_0	n
Value	489.74 MPa	0.02	0.179

5 Numerical Simulation

5.1 Calibration of the Material Parameters

The dog-bone specimen is used to calibrate the material parameters. The mesh size of 0.5 mm × 0.5 mm at critical zone and boundary condition are given in Fig. 4.

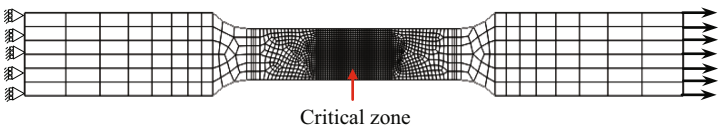

Fig. 4. FEM mesh and boundary condition of the dog-bone specimen

Two parameters of critical damage variable D_{crit} and of softening exponent β would be calibrated by minimizing an objective function $F_{obj}(p)$, defined as follows

$$F_{obj} = \frac{1}{2}\sum_{i=1}^{k}\left(F^i_{\exp} - F^i_{sim}\right)^2 \tag{7}$$

where $p = (p_1, p_2, \ldots, p_i, p_k)$, in which p_i denotes the material parameters, $k = 580$ is the total number of data points $\left(u^i, F^i_{\exp}\right)$ resulted from segmentation of the force-displacement experimental curves, $F_{\exp} - u$. Values of F^i_{sim} are evaluated in simulations at displacement point u^i. The python language (https://www.python.org/) is used to support this process.

The best-fit material parameters that used for predicting of ductile fracture are given in Table 3.

Table 3. The best-fit material parameters of damage model

Parameters	D_{crit}	β
Value	0.55	1.92

The displacement - load curve corresponding to the best-fit material parameters are presented in Fig. 5.

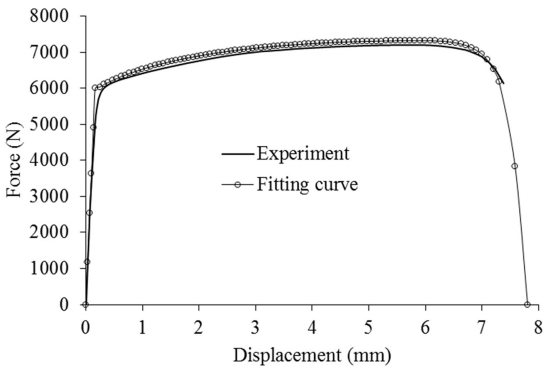

Fig. 5. The displacement – load curve after calibration

5.2 Forming Limit Diagram

In order to obtain various strain states, the difference blank geometries were used to simulate Nakajima test. The blanks were designed in circular shape with the fixed dimension of 185 mm and with the various waist widths W of 30, 55, 70, 90, 120, 145 and 185 mm as Fig. 6(a), after Kami et al. [14]. The thickness of sheet is of 2 mm.

The mesh size at analysis zone is 0.5 mm × 0.5 mm and three element layers through sheet thickness. The element type of 3D, 8-nodes, reduced integration (C3D8R) used for all analyses. Blank is clamped between die and holder by the holding force of F_{hold} = 450 kN to prevent any wrinkling or fail of blank at clamped region. The hemispherical punch, holder and blank are modeled by an assumption of the absolute rigid body with the 3D analytical rigid type. The hemispherical punch radius is 50 mm. Inner diameters of die and holder are 110 mm and 130 mm, respectively while their same outer diameter of 190 mm is used. The contact interaction is assumed to obey Coulomb law, i.e., friction coefficient of 0.03 is applied to the punch-blank contact surface whereas that of 0.1 is taken for die-blank and holder-blank contact surfaces.

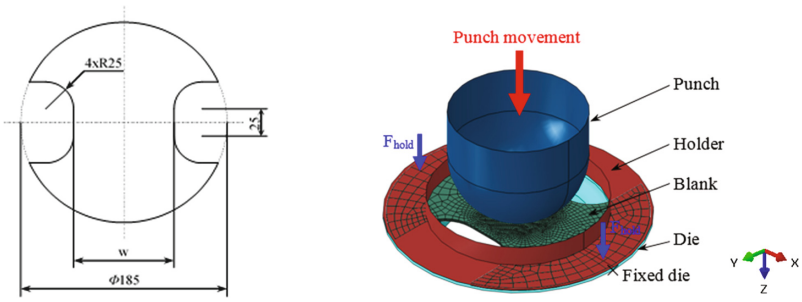

(a) (b)

Fig. 6. Nakajima test: (a) blank and (b) finite element model

The simulation process takes place in 2 steps. In the first step, die and punch are fixed whereas blank is clamped by moving holder in vertical direction and kept by a holding force of 450 kN during this step. In the second step, while the boundary conditions of the first step are maintained, the blank is stretched by moving the punch until its fracture occurs. The deep drawing setup is shown in Fig. 6(b).

Linear Best-Fit Method. Linear best-fit method used to determined FLD curve based on analyzing "thinning rate" of material under plastic deformation due to Volk and Hora [15] proposed. According to this approach, beginning of instable necking can be recognized by two main characteristic effects of concentration plastic deformation and the acceleration of thinning rates at localized necking zone (Fig. 7(a)) where fracture expected to happen (Fig. 7(b)). Particularly, the beginning instability is determined by using two linear fitting lines, one fitted by the stable deformation zone in the beginning (L_1) and one fitted by the "thinning rate" results that just before fracture occurs (L_2). It is noted that fitting line L_1 should be lie in range from 2 mm to 4 mm of punch stroke before specimen failure whereas linear line L_2 is fitted for fit windows size of ± 0,1 mm that corresponding to 3 points in time [16]. The intersection point of these two lines is considered as beginning time of instable necking and the values of major and minor strains at this moment are picked up for constructing FLD curve. To avoid

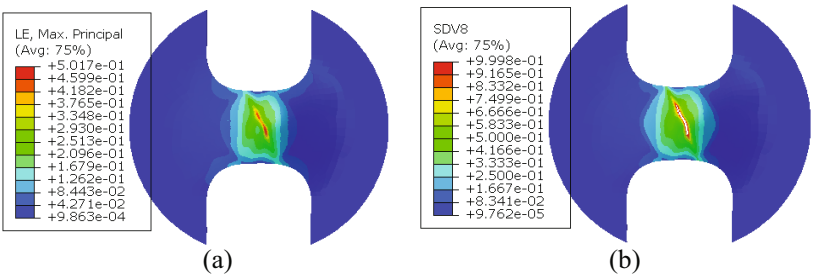

Fig. 7. (a) Contour of principal strain (LE) at necking moment and (b) damage variable (SDV8) at fracture of W55 specimen

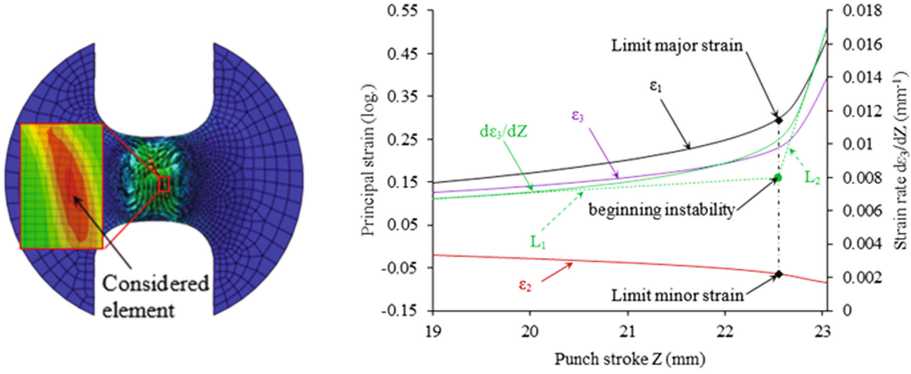

Fig. 8. Determination of limit strain values of W55 specimen using the linear best fit method

unnecessary repetition, Fig. 8 only shows the determination of limit strain values of W55 waist specimen. The principal strain values are extracted from an earliest failure element.

The Cross-Section method. For each specimen, three extracted paths along cross-section consist of a set number of major and minor strain data points are extracted at moment of onset necking that just before fracture occurs, as shown in Fig. 9. With the average strain data of three extracted paths, fitting window is established using the peak major strain location. The size of this window should be lies in a suitable range that limited by inner (purple dash-dot line) and outer (green solid line) boundaries. For further calculation of the fitting window size can be found in ISO 12004-2:2008-part 2. Strain data within the fitting window is then regressed by an inverse parabola, with the parabolic peak generally coinciding with the location of the limit major strain (see Fig. 9). The limit strain values for FLD construction are subsequently obtained basis of this technique.

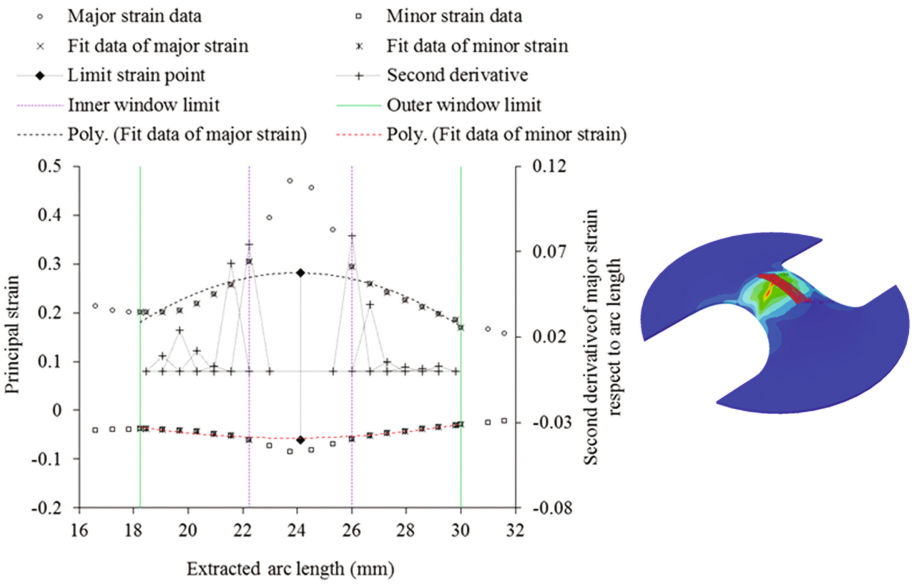

Fig. 9. Determination of limit strain values of W55 specimen using the cross-section method

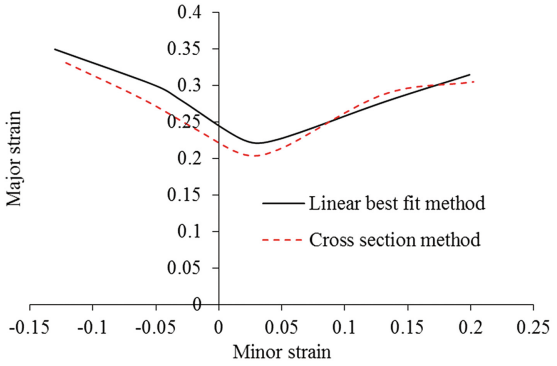

Fig. 10. FLD curve of AA6061-T6 sheet

Figure 10 shows the comparison of the FLD curves between the cross-section method and linear best-fit method for the AA6061-T6 aluminum alloy. In general, the FLD curve obtaining by the linear best fit method shows a shift to little larger values compared to that of cross-section method except mediate state between plane strain and biaxial stretch.

6 Conclusion

In this paper, the FLD curve of the AA6061-T6 aluminum alloy is predicted by a micro-void growth based damage model.

Based on inverse analysis engineering, the best-fit material parameters of damage model are archived by comparing the experimental displacement-load curve with that of numerical simulation. Two methodologies that were recently developed for the determination of the FLD curve are applied to obtain the limit strain values in sheet metal forming. The FLD curve predicted by linear best-fit method is always lower than that of cross-section method in most cases except mediate stretching mode.

With the predicted results of FLD curve in this article the micro-void growth based damage model is promising to apply for predicting ductile fracture of the various sheet metals.

Acknowledgements. This research is funded by Vietnam National University Ho Chi Minh City (VNU-HCM) under grant number C2017-20-05.

References

1. Keeler, S.P., Backofen, W.A.: Plastic instability and fracture in sheets stretched over rigid punches. ASM Trans. Q **56**(1), 25–48 (1963)
2. Goodwin, G.M.: Application of strain analysis to sheet metal forming problems in the press shop, SAE technical paper 0148-7191 (1968)
3. Marziniak, Z., Kuczynski, K.: Limit strain in the process of stretch-forming sheet metals. Int. J. Mech. Sci. **9**, 609–620 (1967)
4. Marciniak, Z., Kuczyński, K., Pokora, T.: Influence of the plastic properties of a material on the forming limit diagram for sheet metal in tension. Int. J. Mech. Sci. **15**(10), 789–800 (1973)
5. Zhang, F., Chen, J., Chen, J.: Effect of through-thickness normal stress on forming limits under Yld2003 yield criterion and MK model. Int. J. Mech. Sci. **89**, 92–100 (2014)
6. Li, H., Wu, X., Li, G.: Prediction of forming limit diagrams for 22MnB5 in hot stamping process. J. Mater. Eng. Perform. **22**(8), 2131–2140 (2013)
7. McClintock, F.A.: A criterion for ductile fracture by the growth of holes. J. Appl. Mech. **35**(2), 363–371 (1968)
8. Rice, J.R., Tracey, D.M.: On the ductile enlargement of voids in triaxial stress fields. J. Mech. Phys. Solids **17**(3), 201–217 (1969)
9. Dung, N.L.: Plasticity theory of ductile fracture by void growth and coalescence. Forsch. Ingenieurwes. **58**(5), 135–140 (1992)
10. Dung, N.L.: Three-dimensional void growth in plastic materials. Mech. Res. Commun. **19**(3), 227 (1992)
11. Ortiz, M., Simo, J.: An analysis of a new class of integration algorithms for elastoplastic constitutive relations. Int. J. Numer. Meth. Eng. **23**(3), 353–366 (1986)
12. Simo, J., Ortiz, M.: A unified approach to finite deformation elastoplastic analysis based on the use of hyperelastic constitutive equations. Comput. Meth. Appl. Mech. Eng. **49**(2), 221–245 (1985)
13. E. ASTM: Standard test methods for tension testing of metallic materials, Annual book of ASTM standards. ASTM (2001)

14. Kami, A., Dariani, B.M., Vanini, A.S., Comsa, D.S., Banabic, D.: Numerical determination of the forming limit curves of anisotropic sheet metals using GTN damage model. J. Mater. Process. Technol. **216**, 472–483 (2015)
15. Volk, W., Hora, P.: New algorithm for a robust user-independent evaluation of beginning instability for the experimental FLC determination. Int. J. Mater. Form. **4**(3), 339–346 (2011)
16. Hotz, W., Merklein, M., Kuppert, A., Friebe, H., Klein, M.: Time dependent FLC determination comparison of different algorithms to detect the onset of unstable necking before fracture. In: Key Engineering Materials, vol. 549, pp. 397–404. Trans Tech Publications (2013)